Atmos. Meas. Tech. Discuss., 8, 8231–8255, 2015
www.atmos-meas-tech-discuss.net/8/8231/2015/
doi:10.5194/amtd-8-8231-2015

Atmospheric Measurement Techniques Discussions

New image measurements of the gravity wave propagation characteristics from a low latitude Indian station

M. Sivakandan[1], **A. Taori**[1], **and K. Niranjan**[2]

[1]National Atmospheric Research Laboratory (NARL), Gadanki, 517112, India
[2]Department of Physics, Andhra University, Visakhapatnam, 530003, India

Received: 17 July 2015 – Accepted: 20 July 2015 – Published: 7 August 2015

Correspondence to: A. Taori (alok.taori@gmail.com)

Published by Copernicus Publications on behalf of the European Geosciences Union.

Abstract

The image observations of mesospheric O(^{1}S) 558 nm have been performed from a low latitude Indian station, Gadanki (13.5° N; 79.2° E) using a CCD based all sky camera system. Based on three years (from year 2012 to the year 2014) of image data during March–April, we characterize the small scale gravity wave properties. We noted 50 strong gravity wave event and 19 ripple events to occur. The horizontal wavelengths of the gravity waves are found to vary from 12 to 42 km with the phase velocity ranging from 20 to 90 km. In most cases, these waves were propagating towards north with only a few occasions of southward propagation. The outgoing longwave radiation data suggest that lower atmospheric convection was most possible reason for the generation of the waves observed in the airglow data.

1 Introduction

The variability in the middle atmospheric parameters is often attributed to be caused due to the energy and momentum deposition by gravity waves (e.g., Fritts and Alexander, 2003). There are many techniques to observe the gravity wave activities in the middle and upper atmosphere, such as radars, lidars, photometers, rockets and satellite observations (e.g., Smith, 2012). However, small scale gravity waves remain the least understood due to the lack of suitable instruments which can provide the scale sizes, propagation direction together with its temporal evolution characteristics. In this regard, ground based airglow imaging is an important tool to estimate the gravity wave signatures. The prime advantage of the imaging is that it provides a 2-dimensional view at the chosen airglow emission altitudes and thus it has the capability to determine the horizontal scales and propagation direction of the gravity waves. Further, at a given place it provides the temporal evolution characteristics of the gravity wave induced oscillations. As the field of view of imagers at mesospheric altitudes may cover a horizontal distance of 200–250 km, such measurements are highly suited for the waves having

AMTD
8, 8231–8255, 2015

small scales (horizontal wavelength < 100 km), short periods (periods < 1 h) and long enough vertical wavelengths (> 10 km) (Liu, 2003).

Since about a decade, capabilities of airglow imaging have been widely utilized to analyze the gravity wave characteristics (e.g., Taylor and Hapgood, 1988; Nakamura et al., 1999; Walterscheid et al., 1999; Medeiros et al., 2003; Ejiri et al., 2003; Kim et al., 2010; Li et al., 2011). Particularly, Nakamura et al. (1999) utilized 18 months of OH imager observations at Shigaraki (34.9° N, 136.1° E) and reported that the gravity waves propagated eastward (westward) in the summer (winter) with horizontal wavelength varying from 10 to 45 km. Medeiros et al. (2003) analyzed 12 months observation at Cachoeira Paulista (23° S, 45° W) and found that gravity waves exhibited preferential propagation directions, with southeast propagation in the summer and northwest in the winter with wavelength range 5–60 km. Using 1 year OH Meinel and OI (557.7 nm) band image data at Rikubetsu (43.5° N, 143.8° E) and Shigaraki (34.9° N, 136.1° E) in Japan from October 1998 to October 1999, Ejiri et al. (2003) reported that gravity waves propagated mostly to the north or northeast during in summer at both sites with wavelengths in the range 10–58 km. However, gravity waves propagated to the west at Rikubetsu and to the southwest at Shigaraki in winter. In a more recent report, Kim et al., (2010) used OH, O_2 and O(^{1}S) (558 nm) data from Mt. Bohyun, Korea (36.2° N, 128.9° E) and found that gravity waves propagate westward during fall and winter and eastward during spring and summer. The wavelengths were found to be in 10–45 km range.

When it comes to the measurements from Indian region, so far, there is only one report by (Lakshmi Narayanan and Gurubaran, 2013), which documents the small scale gravity wave characteristics. It is important to note that being a tropical location, the clear sky availability makes the statistics biased. Therefore, in the present report we have taken the data from 2012 to 2014 during March–April, a pre monsoon season, when the maximum number of cloud free nights are monitored (e.g., Taori et al., 2012) over Gadanki (13.5° N; 79.2° E). We show the gravity wave charactistics for the said duration and that the probable source of these waves lie in the lower atmospheric con-

AMTD
8, 8231–8255, 2015

vective processes with the help of daily mean outgoing Long wave radiation (OLR) obtained from the National Oceanic and Atmospheric Administration (NOAA).

2 Instrumentation and data analysis

The NARL all sky airglow imager (NAI) has been installed at Gadanki (13.5° N, 79.2° E) in March 2012 and since then regular night airglow observations are being carried out during moonless, cloudless clear sky nights. The front optics of NAI uses a fish eye lens having field of view (FOV) 180° (current FOV is limited to 117° due to walls of the room where NAI is placed). Its filter chamber contains three different interference filters, namely 840 nm for OH emission (peak altitude ~ 87 km), 558 nm for O(^{1}S) emission (peak altitude ~ 97 km) and 630 nm for O(^{1}D) emission (peak altitude ~ 250 km). In order to maintain the constant temperature a thermo-electric temperature controller is attached to the filter chamber. After passing through interference filters, to converge the optical rays to the PIXIS-1024B camera system (Princeton Instruments), a camera lens is used. To reduce the dark counts, CCD is thermoelectrically cooled to −70 °C before the operation, The final image captured by the CCD camera is stored on the computer hard disk for further analysis. In the present set-up, we bin the images for 2 × 2 pixels making an effective 512 × 512 super pixel image on the chip to enhance the signal-to-noise ratio. Depending on the compromise among the background luminosity, interference filter transmission and actual airglow brightness, at present exposure time of the filters are like this 15 s for OH and 110 s for both, O(^{1}S) and O(^{1}D) emission monitoring. Further details of the NAI are elaborated elsewhere (Taori et al., 2013).

In the present study, we use 3 years (2012–2014) of O(^{1}S) airglow imager data in the months of March and April (spring equinox months). From these three years of observations, we could get 32 clear sky night data. From raw images we have cropped the images for 90° full field of view to avoid the nonlinear scales at the edges arising due to the lens curvature effect. Further, we unwrapped the images for Barrel distortions to further linearize the scales. At last, we enhance the image by contrast adjustment

AMTD
8, 8231–8255, 2015

(for better visibility). In order to remove the stars we used the median filters. In thus obtained, processed images, continuous bright and dark band which sustain in more than three consecutive images are considered as the structure depicting a wave event. This analysis is performed on all the data. We note that in 32 days of data, 69 clear wave events were prominent. Among these 69 events, 19 events did not show any phase propagation and were moving with its background. Those wave events are considered as ripples (which may be arising due to Kelvin Helmholtz instability occurring due to the wave dissipation) and thus have not been considered as propagating gravity waves. An example of a gravity wave event is shown in Fig. 1. In this figure, red lines are drawn close to the bright bands to elaborate the wave fronts. The propagation is identified by cross correlating the position of these fronts from one image to another in consecutive images. Further, the line connecting to the normal point of these fronts is considered to be the angle of propagation (shown as a yellow line with an arrow indicating the direction of propagation). The estimate of propagation angle is done by measuring the angle between the yellow line with the horizontal line parallel to the east direction. In order to get the horizontal wavelength of the observed wave event, we took the perpendicular pixels of wave phase (yellow colored arrows) and plot the gray count values. The distance between two peaks provides the horizontal wavelength estimates (in this particular wave event horizontal wavelength is estimated to be ~ 14 km). To calculate the phase velocity (Vp = displacement/time-difference) of the wave event, first we calculate the phase displacement of the wave from one image to the other (for example, if the position of a wave phase is (x_1, y_1) in the first image and in the second image the position is (x_2, y_2), then the displacement is defined as, $d = \sqrt{(x_2 - x_1)^2 + (y_2 - y_1)^2}$). In the case shown, the observed phase velocity is estimated to be $\sim 23\,\mathrm{m\,s^{-1}}$ and the estimated angle of wave propagation is $\sim 55^{\circ}$.

We performed this analysis on the full data set (i.e., 50 wave events of which 21 events in the year 2012, 5 events in the year 2013 and 24 events in the year 2014) and wave characteristics obtained as explained above are presented in this report.

AMTD
8, 8231–8255, 2015

3 Results and discussion

First, we present the composite results for the years 2012–2014 to show the overview of the results. We note that horizontal wavelengths of the observed wave events are found to vary from 10 to 45 km (Fig. 2). Among this distribution, we note that about half of the wave events have their horizontal wavelengths in 10–25 km range and 22 % wave events are noted in 30–35 km wavelength range. It is evident from Fig. 2 that more than 90 % wave events are having a wavelength less than 35 km. The estimated horizontal phase velocity distribution of the observed wave events is shown in Fig. 3. It is noteworthy that the phase velocity vary from 20 to 90 $m\,s^{-1}$. We note that ~ 78 % of the wave events show the phase velocity less than 50 $m\,s^{-1}$. Using the observed horizontal wavelength and phase speed we have calculated the periodicity of the observed wave events which is shown in Fig. 4. The periods of observed gravity waves are found to be in 4 to 20 min range. We also note that about 90 % waves have their periods in 6 to 15 min range with only 1 % of waves having their periods more than 15 min. When it comes to the direction of propagation of the observed wave events, we observed that most of the times they propagate towards north (Fig. 5) with only few events showing southward propagation. In this figure, red colored arrows indicate the wave propagation angle in the month of March and the blue color arrows indicate the wave propagation angle in the month of April for the years 2012, 2013 and 2014. The dotted circles denote the horizontal phase velocity of the observed wave events with an interval of 20 $m\,s^{-1}$. As the waves propagate away from their source regions (e.g., Pautet et al., 2005), it is prudent to suggest that the wave generations must be located somewhere in the south of the measurement location. An earlier report from Indian subcontinent by (Lakshmi Narayanan and Gurubaran, 2013) from Tirunelveli (8.7° N), based on data corresponding to the year 2007 suggested that during equinox season waves mainly propagate towards the north which further confirms our assertion.

A comparison of our results with a few earlier investigations of gravity wave characteristics using similar methods (i.e., airglow imaging) is made in Table 1 (please note

AMTD
8, 8231–8255, 2015

that the list is not exhaustive). It is noteworthy that although the wavelengths, phase velocity and observed wave periods are within the range reported by most of the investigators, there are differences from (Ding et al., 2004) and (Suzuki et al., 2009) where they observe significantly larger wavelengths. The reason behind this deviation may be associated with the source properties having totally different forcing characteristics.

As the most of the small scale waves observed in mesosphere have their origin in lower atmospheric processes such as tropospheric convection, wind shear, wave-wave interaction or secondary wave generation (e.g., Alexander, 1996; Holton and Alexander, 1999; Pandya and Alexander, 1999; Piani et al., 2000; Fritts and Alexander, 2003; Taori et al., 2012; Pramitha et al., 2015). Numerous modelling as well as experimental evidences over equatorial latitudes suggest that most of the small scale waves with periods less than an hour have their sources in convective processes (e.g., Holton and Alexander, 1999; Horinouchi et al., 2003; Nakamura, 2003; Pautet et al., 2005). Of the particular relevance to our observations is the report by Pautet et al., (2005) where based on the 19 wave events it was clearly shown that waves were generated by the convection and propagated away from their sources (convective clouds). To investigate whether convection and associated processes are the prime potential sources for the perturbations noted in the middle atmosphere and ultimately reflected in the upper mesospheric altitudes, we look into (a) propagation direction and phase velocity of waves from year to year, and (b) average the daily mean NOAA-OLR for the days when airglow observations were made. We elaborate these events in the following.

Figure 6 shows the propagation direction and phase velocity of the wave events noted during March–April 2012. Similar to the Fig. 5, red colored arrows indicate the wave propagation angle in the month of March and the blue color arrows indicate the wave propagation angle. The dotted circles denote the horizontal phase velocity of the observed wave events with an interval of $20\,m\,s^{-1}$. We note that most often the waves are propagating to the northwestward. Few waves were travelling towards the northeast while only 2 wave events having their propagation towards south. The average of daily mean OLR data during the observations is plotted in Fig. 7. The left map shows

AMTD
8, 8231–8255, 2015

the averaged OLR values for March month while the right map is for April 2012. The location of measurement is shown as the filled black circle. One may note that during the March month there is a deep convection (OLR < 200) occurring at the southeast location of the map hence the waves propagating away from these sources shall have the propagation in the north-west direction which is consistent with the observations. It is interesting to note that during April month apart from the deep convection at the southeast location, there is a convective patch on the southwest side of the map. In this regard, observations suggesting that in the April month waves propagated in the north-east and northwest directions (in Fig. 6) are consistent with the fact that their sources were associated with the convective plumes noted in the OLR data. There are two wave events which show southward propagation (on 27 March 2012). We plotted the daily mean OLR data separately for this night in Fig. 8. We note that there was some convective process occurring in northern locations. It is also important to note that there were some isolated convective process at 20° N, 76° E (source: http://www.mosdac.gov.in) which may have triggered these waves. It is important to note that we could observe only those events which could overcome the wind filtering mechanisms. Typical zonal and meridional winds during March–April months over Tirunelveli (8.7° N,77.° E) are reported to be ∼ 15 and 18 $m\,s^{-1}$ (Sivakandan et al., 2015) in 85–100 km altitude range, and also that Horizontal Wind Model (HWM-07) wind estimates also suggest the maximum winds to be less than 20 $m\,s^{-1}$ at these altitudes. Thus, waves having their phase velocity more than 20 $m\,s^{-1}$ will not be blocked by the horizontal winds and may propagate to their preferred directions governed by the source properties. We believe that this is the reason we noted the waves have their phase velocity more than 20 $m\,s^{-1}$.

The NAI could not be operated during March 2013 however, the propagation and phase velocity of the wave events noted in April 2013 are shown in Fig. 9. We note that out of 5 wave events, 3 waves were propagating to the northeast directions, 1 was propagating northwestward while 1 wave was propagating to the southeast. Important to note is that all the waves had their phase velocity higher than 20 $m\,s^{-1}$. The OLR data corresponding to April 2013 events are plotted in Fig. 10 where it is clear that

AMTD
8, 8231–8255, 2015

there were convective regions in the southern side of the measuring site which most possibly triggered the waves which were propagating to the northeast and northwest directions with one of the event propagating to southeast direction triggered by some other mechanism may possibly be by wind shears (Pramitha et al., 2015).

The polar plot depicting the gravity wave propagation direction and phase velocity corresponding to the year 2014 is shown in Fig. 11. This year wave directions show deviations compared to the year 2014. In year 2012 waves propagated dominantly to the northwest while in 2014 waves are moving towards northeast with a substantial number of waves in southward directions. The OLR corresponding to the March and April 2014 are shown in Fig. 12a and b. It is noteworthy that there are convective processes occurring in southward as well as northward directions and thus the waves triggered by these sources are reflected in our measurements. However, the waves propagating almost in zonal directions are not expected to be of convective origin. This also suggests that other processes may be responsible for these waves though convection may be the prime source of gravity waves.

4 Summary

The image measurements of 558 nm O(^{1}S) nightglow during the spring season over Indian low latitudes show conspicuous signatures of upper mesospheric waves. The horizontal wavelengths ranged from 10 to 45 km and were mostly found to propagate towards the north side of the location of the measurements. Over the Indian subcontinent, often the lower atmospheric convection activities occur at the southern side of the location which we have also noted in the OLR data. The directions of wave propagation were found to be consistent with the source being in the south, which suggest that lower atmospheric convection and associated processes are behind the generation of the observed waves. The direction and wavelength of the gravity waves are considered important from neutral-ion coupling as the signatures of gravity waves in the E-region have their consequences on the upper atmospheric processes (i.e., spread-F) whose

AMTD
8, 8231–8255, 2015

day to day variability are least understood (e.g., Makela and Otsuka, 2012). Future studies will aim at identifying the exact sources of the observed waves and role of the source properties on gravity wave energy and spectrum observed in the mesosphere.

Acknowledgements. The present work is supported by the Department of Space, Government of India. We acknowledge the help of Mr. Liyakat Basha, V. Kamalakar and R. Goenka for their help in carrying out night airglow measurements. We thank Ms. C. A. Smith of NOAA Earth System Research Laboratory for providing the interpolated OLR data (source: www.esrl.noaa.gov/psd/data/gridded/data.interp_OLR.html).

References

Alexander, J.: A simulated spectrum of convectively generated gravity waves: propagation from the tropopause to the mesopause and effects on the middle atmosphere, J. Geophys. Res., 101, 1571–1588, doi:10.1029/95JD02046, 1996.

Ding, F., Yuan, H., Wan, W., Reid, I. M., and Woithe, J. M.: Occurrence characteristics of medium-scale gravity waves observed in OH and OI nightglow over Adelaide (34.5° S, 138.5° E), J. Geophys. Res.-Atmos., 109, 1–10, doi:10.1029/2003JD004096, 2004.

Ejiri, M. K.: Statistical study of short-period gravity waves in OH and OI nightglow images at two separated sites, J. Geophys. Res., 108, 1–12, doi:10.1029/2002JD002795, 2003.

Fritts, D. C. and Alexander, M. J.: Gravity wave dynamics and effects in the middle atmosphere, Rev. Geophys., 41, 1003, doi:10.1029/2001RG000106, 2003.

Holton, J. R. and Alexander, M. J.: Gravity waves in the mesosphere generated by tropospheric convention, Tellus B, 51, 45–58, doi:10.3402/tellusa.v51i1.12305, 1999.

Horinouchi T., Pawson, S., Shibata, K., Langematz, U., Manzini, E., Giorgetta, M. A., Sassi, F., Wilson,R. J., Hamilton, K., Grandpre, J. De, and Scaife A. A.: Tropical cumulus convection and upward-propagating waves in middle-atmospheric GCMs, J. Atmos. Sci., 60, 2765–2782, doi:10.1175/1520-0469(2003)060<2765:TCCAUW>2.0.CO;2, 2003.

Kim, Y. H., Lee, C., Chung, J. K., Kim, J. H., and Chun, H. Y.: Seasonal variations of mesospheric gravity waves observed with an airglow all-sky camera at Mt. Bohyun, Korea (36° N), J. Astron. Sp. Sci., 27, 181–188, doi:10.5140/JASS.2010.27.3.181, 2010.

AMTD
8, 8231–8255, 2015

Lakshmi Narayanan, V. and Gurubaran, S.: Statistical characteristics of high frequency gravity waves observed by OH airglow imaging from Tirunelveli (8.7° N), J. Atmos. Sol.-Terr. Phy., 92, 43–50, doi:10.1016/j.jastp.2012.09.002, 2013.

Li, Q., Xu, J., Yue, J., Yuan, W., and Liu, X.: Statistical characteristics of gravity wave activities observed by an OH airglow imager at Xinglong, in northern China, Ann. Geophys., 29, 1401–1410, doi:10.5194/angeo-29-1401-2011, 2011.

Liu, A. Z.: and OH airglow perturbations induced by atmospheric gravity waves, J. Geophys. Res., 108, 4151, doi:10.1029/2002JD002474, 2003.

Makela, J. J. and Otsuka, Y.: Overview of nighttime ionospheric instabilities at low- and mid-latitudes: coupling aspects resulting in structuring at the mesoscale, Space Sci. Rev., 168, 419–440, 2012.

Medeiros, A. F., Taylor, M. J., Takahashi, H., Batista, P. P., and Gobbi, D.: An investigation of gravity wave activity in the low-latitude upper mesosphere: propagation direction and wind filtering, J. Geophys. Res., 108, 1–8, doi:10.1029/2002JD002593, 2003.

Nakamura, T.: Mesospheric gravity waves over a tropical convective region observed by OH airglow imaging in Indonesia, Geophys. Res. Lett., 30, 1999–2002, doi:10.1029/2003GL017619, 2003.

Nakamura, T., Higashikawa, A., and Tsuda, T.: Seasonal variation of gravity waves observed with an OH CCD imager at Shigaraki (35° N, 136° E), Japan, Adv. Space Res., 24, 561–564, doi:10.1016/S0273-1177(99)00201-X, 1999.

Pandya, R. E. and Alexander, M. J.: Linear stratospheric gravity waves above convective thermal forcing, J. Atmos. Sci., 56, 2434–2446, doi:10.1175/1520-0469(1999)056<2434:LSGWAC>2.0.CO;2, 1999.

Pautet, P. D., Taylor, M. J., Liu, A. Z., and Swenson, G. R.: Climatology of short-period gravity waves observed over northern Australia during the Darwin Area Wave Experiment (DAWEX) and their dominant source regions, J. Geophys. Res.-Atmos., 110, 1–13, doi:10.1029/2004JD004954, 2005.

Piani, C., Durran, D., Alexander, M. J., and Holton, J. R.: A numerical study of three-dimensional gravity waves triggered by deep tropical convection and their role in the dynamics of the QBO, J. Atmos. Sci., 57, 3689–3702, doi:10.1175/1520-0469(2000)057<3689:ANSOTD>2.0.CO;2, 2000.

Pramitha, M., Venkat Ratnam, M., Taori, A., Krishna Murthy, B. V., Pallamraju, D., and Vijaya Bhaskar Rao, S.: Evidence for tropospheric wind shear excitation of high-phase-speed

AMTD
8, 8231–8255, 2015

gravity waves reaching the mesosphere using the ray-tracing technique, Atmos. Chem. Phys., 15, 2709–2721, doi:10.5194/acp-15-2709-2015, 2015.
Sivakandan, M., Taori, A., Sathishkumar, S., and Jayaraman, A.: Multi-instrument investigation of a mesospheric gravity wave event absorbed into background, J. Geophys. Res., 120, 3150–3159, doi:10.1002/2014JA020896, 2015.
Smith, A. K.: Global dynamics of the MLT, Surv. Geophys., 33, 1177–1230, doi:10.1007/s10712-012-9196-9, 2012.
Suzuki, S., Shiokawa, K., Liu, A. Z., Otsuka, Y., Ogawa, T., and Nakamura, T.: Characteristics of equatorial gravity waves derived from mesospheric airglow imaging observations, Ann. Geophys., 27, 1625–1629, doi:10.5194/angeo-27-1625-2009, 2009.
Taori, A., Raizada, S., Ratnam, M. V., Tepley, A. C., Nath, D., and Jayaraman, A.: Role of tropical convective cells in the observed middle atmospheric gravity wave properties from two distant low latitude stations, Earth Sci. Res. J., 1, 87–97, doi:10.5539/esr.v1n1p87, 2012.
Taori, A., Jayaraman, A., and Kamalakar, V.: Imaging of mesosphere-thermosphere airglow emissions over Gadanki (13.5° N, 79.2° E) – first results, J. Atmos. Sol.-Terr. Phy., 93, 21–28, doi:10.1016/j.jastp.2012.11.007, 2013.
Taylor, M. J. and Hapgood, M. A.: Identification of a thunderstorm as a source of short period gravity waves in the upper atmospheric nightglow emissions, Planet. Space Sci., 36, 975–985, doi:10.1016/0032-0633(88)90035-9, 1988.
Walterscheid, R. L., Hecht, J. H., Vincent, R. A., Reid, I. M., Woithe, J., and Hickey, M. P.: Analysis and interpretation of airglow and radar observations of quasi-monochromatic gravity waves in the upper mesosphere and lower thermosphere over Adelaide, Australia (35° S, 138° E), J. Atmos. Sol.-Terr. Phy., 61, 461–478, doi:10.1016/S1364-6826(99)00002-4, 1999.

AMTD
8, 8231–8255, 2015

Table 1. Comparison of the present results with the small scale wave measurements made by earlier investigators from other latitudes using airglow imaging.

Station	Latitude, Longitude	Horizontal wavelength (km)	Phase speed ($m s^{-1}$)	Observed period (min)	References
Shigaraki	35° N, 136° E	5–60	0–100	0–30	Nakamura et al. (1999)
Shigaraki	35° N, 136° E	5–60	0–120	0–50	Takahashi et al. (1999)
Rikubetsu	43.5° N, 143.8° E	10–42 (OH) 10–58 (O^1S)	0–100 10–110		Ejiri et al. (2003)
Cachoeira Paulista	23° S, 45° W	5–60	10–80	6–34	Medeiros et al. (2003)
Tanjungsari	6.9° S, 107.9° E	3–80	10–95	5–13	Nakamura et al. (2003)
Darwin	12.4° S, 131° E	20–90	0–90		Suzuki et al. (2004)
Buckland Park	34.5° S, 138.5° E	20–200	20–250	40–240	Ding et al. (2004)
Cariri	7.4° S, 36.5° W	5–40	0–90	5–30	Medeiros et al. (2007); Wrasse et al. (2006)
Resolute Bay,	74.7° N, 265.1° E	10–70	10–110		Suzuki et al. (2009a)
Kototabang	0.2° S, 100.3° E	25–95	5–125		Suzuki et al. (2009b)
Mt. Bohyun, Korea	36.2° N, 128.9° E	10–45	0–80	5–45	Kim et al. (2010)
Xinglong	40.2° N, 117.4° E	10–55	10–100	2–20	Li et al. (2011a)
Maui	20.7° N, 156.3° W	10–120	0–150	5–30	Li et al. (2011b)
Syowa Station	69° S, 0–40° E	10–60	0–150	3–65	Matsuda et al. (2014)
Tirunelveli	8.7° N, 77.8° E	5–45	10–140	3–20	Lakshmi Narayanan and Gurubaran, (2013)
Gadanki	13.5° N, 79.2° E	12–45	20–90	4–20	**Present Study**

AMTD
8, 8231–8255, 2015

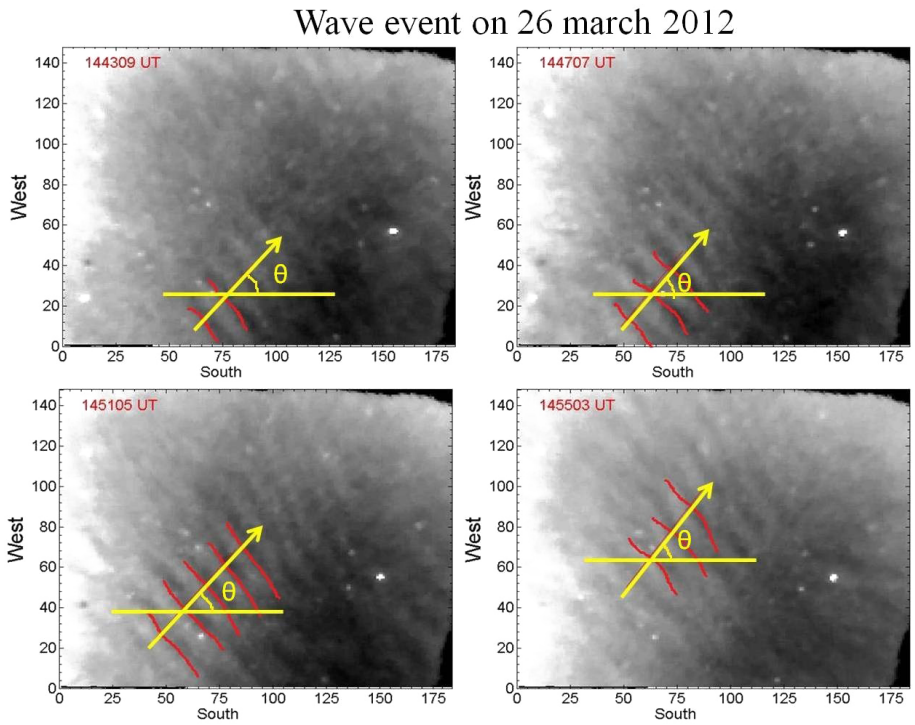

Figure 1. A sample figure depicting the gravity wave signatures. One may see the propagation of features. The red hand sketches elaborate the dominant wave fronts noted while the yellow arrows reveal their propagation direction at an angle Θ.

AMTD
8, 8231–8255, 2015

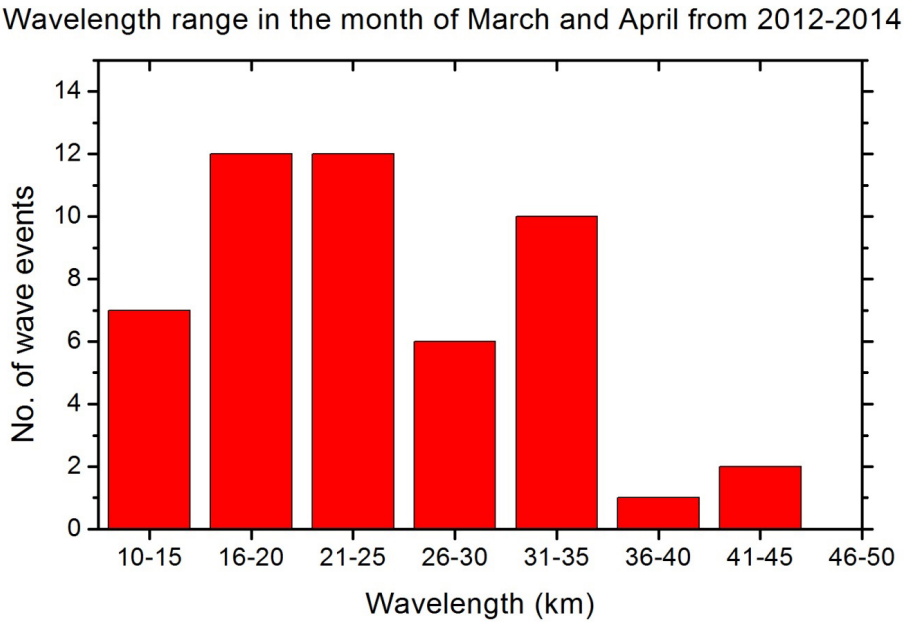

Figure 2. The distribution of horizontal wavelengths of the observed waves during March and April months from the year 2012 to 2014.

AMTD
8, 8231–8255, 2015

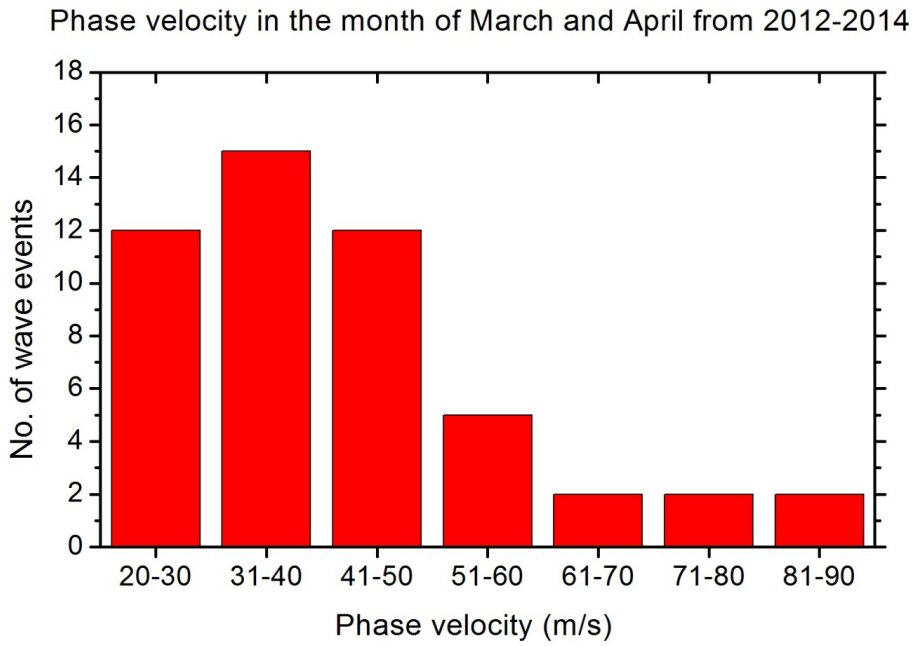

Figure 3. The distribution of the observed phase velocity of waves during March and April months from the year 2012 to 2014.

AMTD
8, 8231–8255, 2015

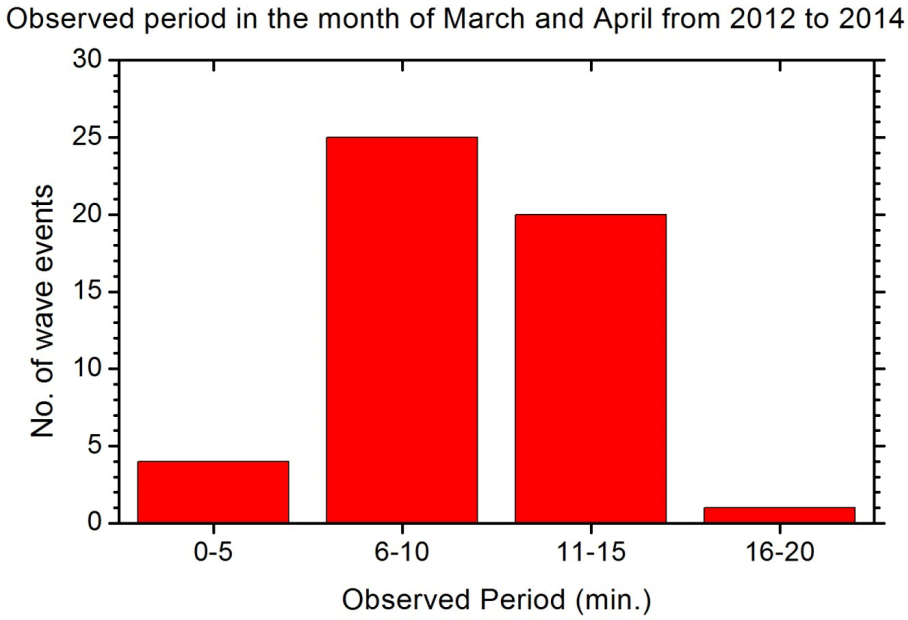

Figure 4. The distribution of observed periods of the waves during March and April months for the years 2012–2014.

AMTD
8, 8231–8255, 2015

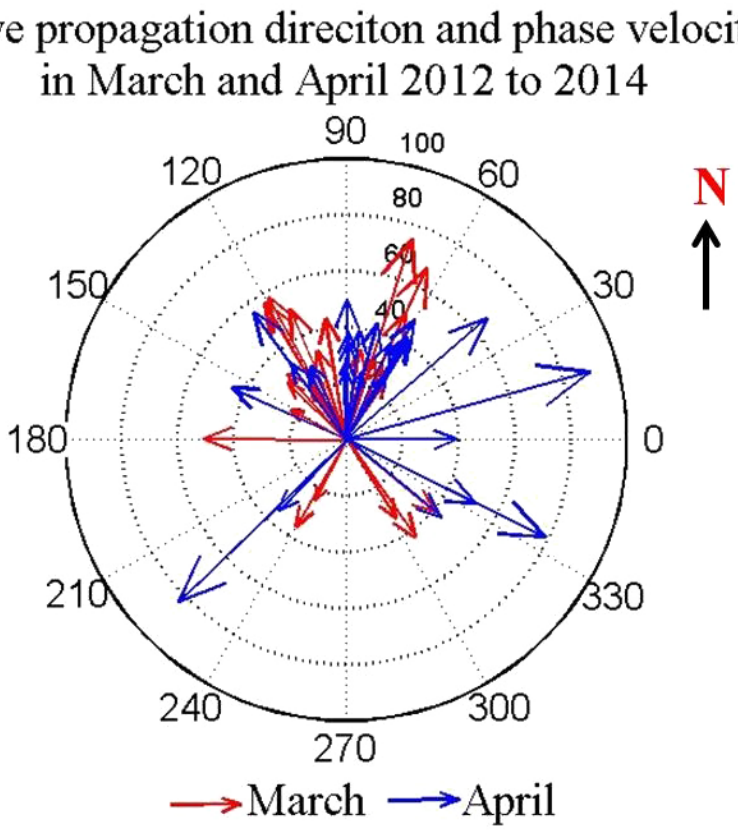

Figure 5. The composite polar plot depicting the observed phase speed and direction of horizontal propagation of gravity waves observed during March–April months during the years 2012–2014. The red color arrows indicate March month events while blue arrows show the events noted in April month. In this figure 0° belongs to the east and the inner dotted circles indicate the horizontal phase speed of the observed wave at an interval of 20 m s^{-1}.

AMTD
8, 8231–8255, 2015

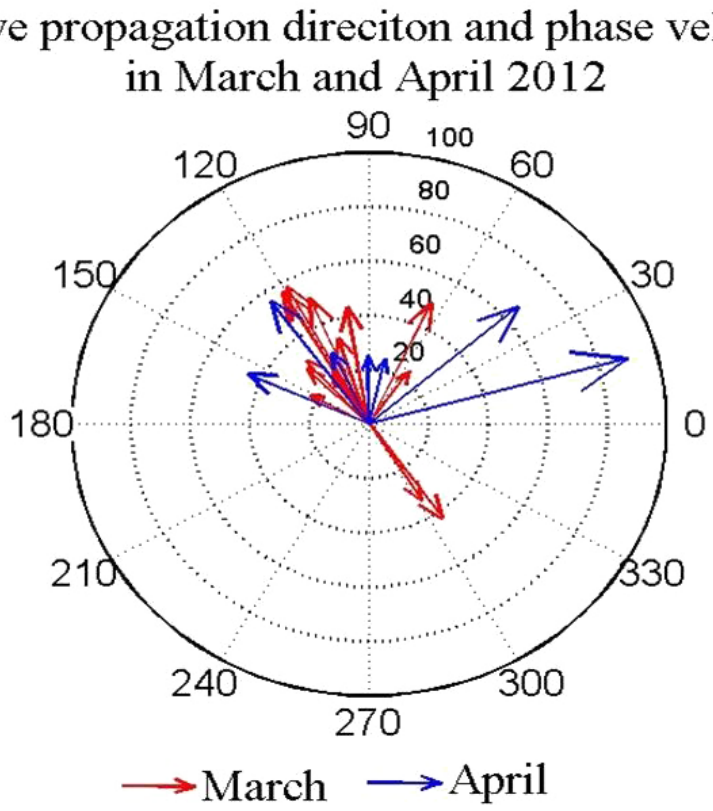

Figure 6. Same as Fig. 5 but only for the year 2012.

AMTD
8, 8231–8255, 2015

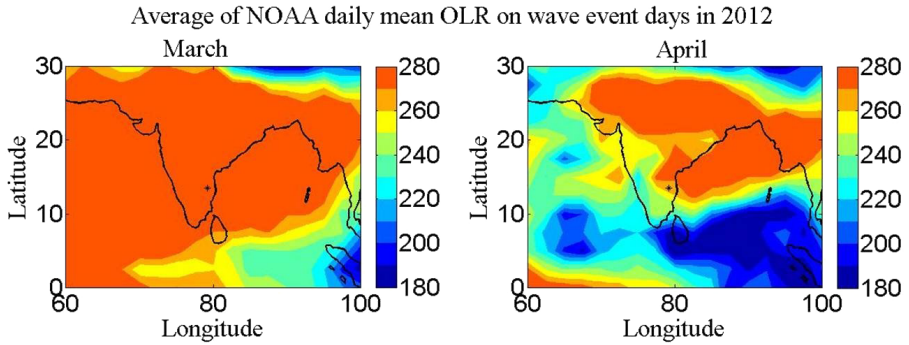

Figure 7. The average of daily mean OLR for the days when waves were observed in airglow image data in March and April 2012. The location of measurement is shown as filled circle in each map.

AMTD
8, 8231–8255, 2015

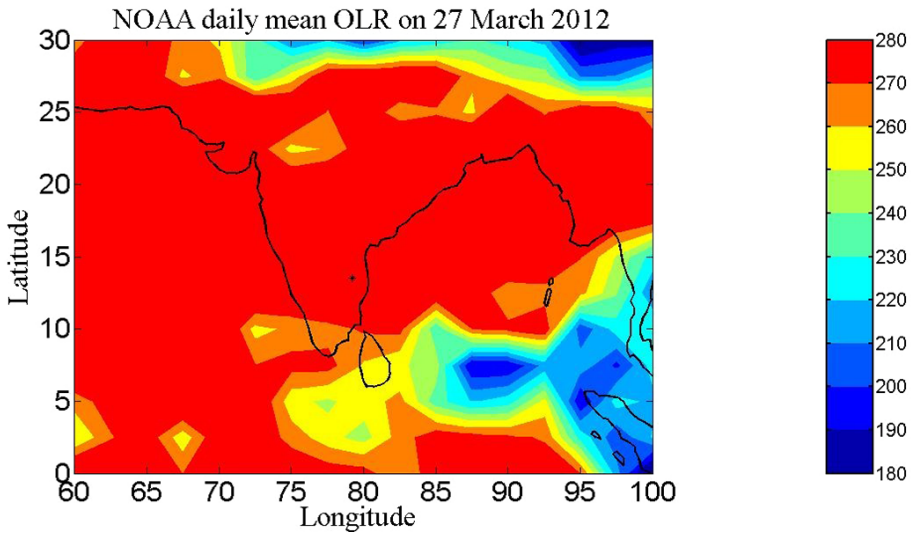

Figure 8. The daily mean OLR data for 27 March 2012. Note the occureence of convective events at northern Indian locations.

AMTD
8, 8231–8255, 2015

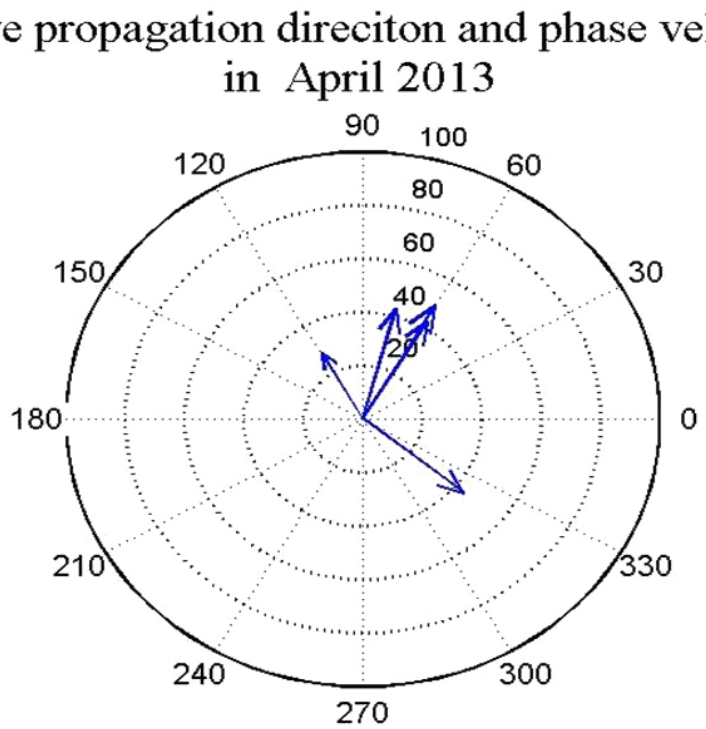

Figure 9. Same as Fig. 5 but for the year 2013.

AMTD
8, 8231–8255, 2015

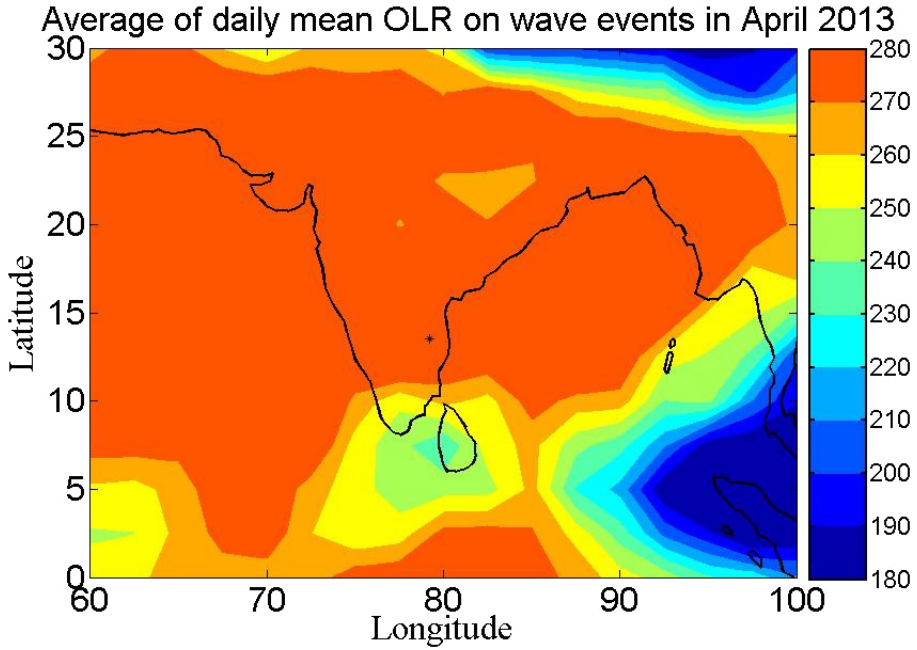

Figure 10. Same as Fig. 7 but for the year 2013.

AMTD
8, 8231–8255, 2015

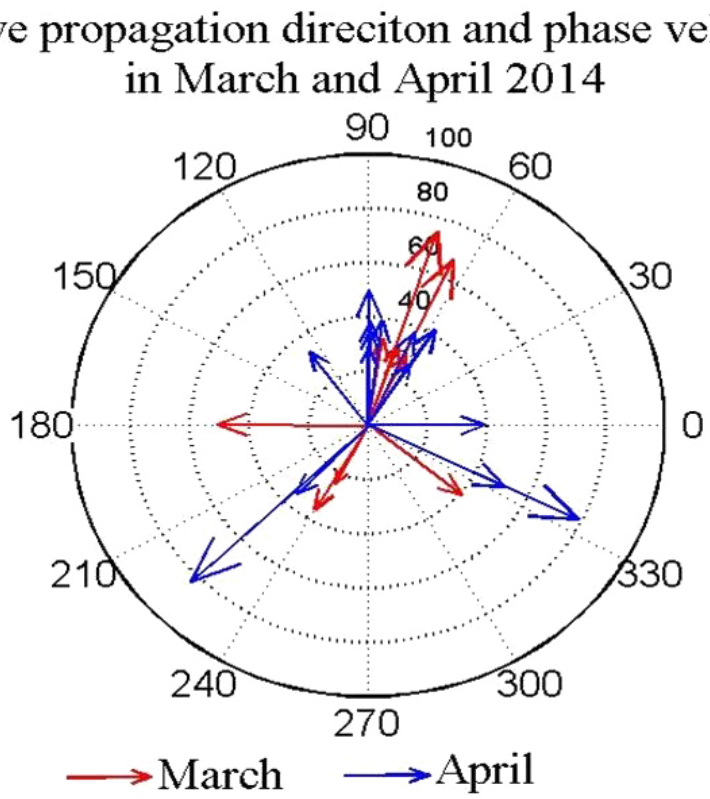

Figure 11. Same as Fig. 5 but for the year 2014.

AMTD
8, 8231–8255, 2015

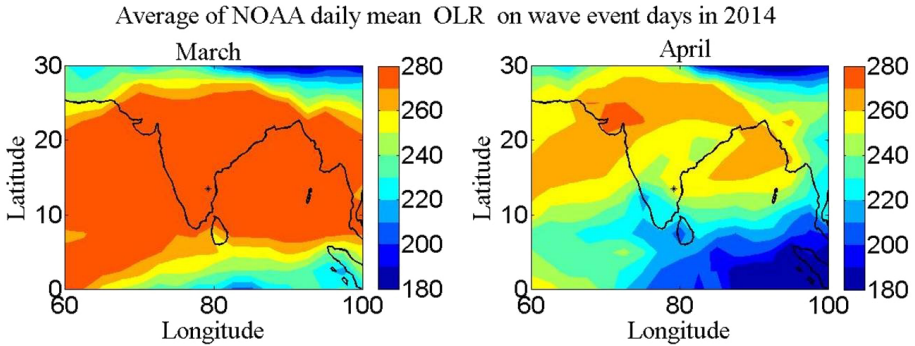

Figure 12. Same as Fig. 7 but for the year 2014.

AMTD
8, 8231–8255, 2015